

Quantum order by disorder in a spin-one frustrated magnet on the kagome lattice

Sergei V. Isakov¹ and Yong Baek Kim²

¹ *Institute for Theoretical Physics, ETH Zürich, CH-8093 Zürich, Switzerland*

² *Department of Physics, University of Toronto, Toronto, Ontario M5S 1A7, Canada*

(Dated: November 3, 2018)

We study the XXZ spin-one quantum magnet on the kagome lattice as an example where quantum fluctuations on highly degenerate classical ground states lead to various exotic quantum ground states. Previous studies have predicted several quantum phases, but different analytical approaches do not necessarily lead to the same physical picture. In this work, we use Quantum Monte Carlo computations to critically examine some of the predictions made in the string-net mean-field theory and the degenerate perturbation theory combined with duality analysis and effective field theory. It is found that the resulting phase diagram differs from some of the previous predictions. Further implications of our results to different analytical approaches are discussed.

PACS numbers: 75.10.Jm, 71.27.+a, 75.40.Mg

I. INTRODUCTION

Macroscopic degeneracy of classical ground states in frustrated magnets is a fertile ground for emergence of unusual quantum ground states such as spiral magnetic order, quantum spin liquid, and valence bond solid (VBS) that occur via quantum fluctuations.¹ Any perturbation on the degenerate classical ground states, however, is inherently strong and there may also be more than one competing ground states that are extremely close in energy. The situation is very reminiscent of quantum Hall states that emerge from highly degenerate Landau levels. This is indeed one of the reasons why identification of true quantum ground state in frustrated magnets is such a difficult task.

Different kinds of non-perturbative analytical approaches have been proposed in literature to understand this quantum order (or disorder) by disorder phenomena. These approaches include various degenerate perturbation theories,² duality analysis combined with effective field theories,^{1,2} and string net condensation picture.³ Since different approaches may not necessarily lead to the same conclusion, it is important to understand the limitations of various approaches. One useful way to obtain such information is doing unbiased numerics by appropriately choosing concrete examples where predictions from different approaches may vary.

Here we consider the following spin-one XXZ model on the kagome lattice as such an example.

$$H = -J_{\perp} \sum_{\langle ij \rangle} (S_i^x S_j^x + S_i^y S_j^y) + J_z \sum_{\langle ij \rangle} S_i^z S_j^z + D \sum_i (S_i^z)^2, \quad (1)$$

where $J_{\perp}, J_z, D > 0$, the first two sums run over the nearest neighbors on the kagome lattice, and D is the strength of the single-ion anisotropy. This model is also equivalent to a boson model with nearest neighbor repulsive interaction where boson occupation number can only assume 0, 1, 2. Previously two different analytical approaches have been used to study the phase diagram of this model. Using degenerate perturbation theory and

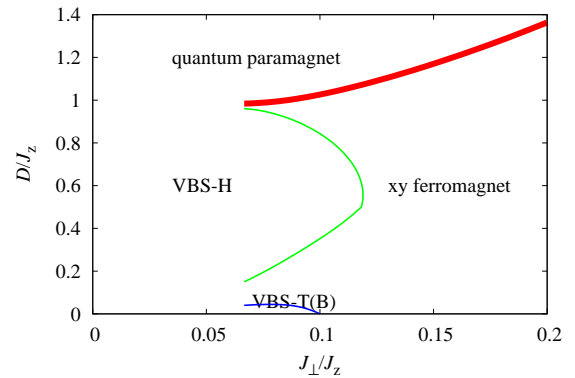


FIG. 1: (color online). The schematic phase diagram. First order phase transitions are denoted by thin lines (blue and green online) and a continuous phase transition is denoted by a thick line (red online).

mapping to a dimer model combined with duality analysis, Xu and Moore^{4,5} predict that there exist three different phases: an XY ferromagnetic phase for $J_{\perp} \gg J_z, D$, a plaquette valence bond solid (VBS-H) phase with resonating hexagons for $J_{\perp} \ll D < J_z$, and a gapped “photon” (quantum paramagnetic) phase for $J_{\perp} \ll J_z < D$. The gapped “photon” phase is a descendant of an unstable two-dimensional quantum spin liquid phase with linearly dispersing neutral “photon” modes. It was also predicted that there would be a direct transition between VBS-H and a gapped “photon” phase. Using a quite different approach, Levin and Wen⁶ proposed a mean-field theory where a class of variational wavefunctions based on the so-called “string-net” picture was used to map out the global phase diagram. While they also predict the existence of a plaquette phase as well as a gapped “photon” phase, their plaquette phase is characterized by frozen spin configurations and this frozen plaquette (FP) phase is different from VBS-H in lattice and spin symmetries.⁶ In this string-net mean-field theory, the “photon” phase corresponds to the string-net

condensed phase⁶ and the unstable two-dimensional spin liquid phase mentioned above. This “photon” phase was found in a narrow region around $J_z \sim D$ if one ignored the nonperturbative instanton contribution. The “photon” excitation acquires a finite gap, however, due to the instanton effect in 2+1 dimensions.^{6,7} The resulting state is an ordinary quantum paramagnetic state.

In this work, we map out the phase diagram of the model given by Eq. 1 using quantum Monte Carlo method. We use a plaquette generalization⁸ of the stochastic series expansion algorithm.⁹ We consider only the parameter region $J_\perp > 0$, $J_z > 0$, and $D > 0$. The schematic phase diagram is shown in Fig. 1. First, we find that a plaquette ordered VBS phase indeed arises and it is the VBS-H phase, not the FP. In addition to the phases discussed in the previous works, we also find an additional phase with resonating lattice units for small values of D/J_z and J_\perp/J_z . The ground state in this region is either a phase with resonating triangles (VBS-T) or a phase with resonating bow ties (VBS-B). It was argued in Ref. 5 that there should be a direct continuous transition from the VBS-H phase to the paramagnetic (gapped “photon”) phase. We do not observe such a transition for $J_\perp/J_z \gtrsim 0.08$. However, we cannot fully rule out the possibility of a direct VBS-H-paramagnet phase transition at even smaller values of J_\perp/J_z .

The rest of the paper is organized as follows. In Section II, we will discuss the details of the phase diagram and properties of all the phases discovered in the numerics. Here we also discuss the difference between our results and the predictions of previous works. We discuss the implications of our results to various analytical approaches in Section III.

II. CONSTRUCTION OF THE PHASE DIAGRAM

A. VBS-H phase

We begin with the analysis of the VBS-H phase that is found in a wide lobe as shown in Fig. 1. This phase has plaquette order. Two different plaquette phases were proposed previously for this region of parameters. In the plaquette phase (VBS-H) predicted by Xu and Moore,^{4,5} spins resonate on a third of the total number of hexagons. These spins have $\langle S_i^z \rangle = b/2$ around resonating hexagons, where b is some number. The rest of the spins is fixed to $\langle S_i^z \rangle = -b$. In the frozen plaquette phase (FP) predicted by Levin and Wen,⁶ spins are frozen on a third of all the hexagons with alternating values of $\langle S_i^z \rangle = \pm a$ around those frozen hexagons; the rest of the spins has $\langle S_i^z \rangle = 0$.⁶ Thus, these two phases break Ising and lattice symmetries in different ways. Note that these two phases can also be distinguished by the distribution function of $\langle S_i^z \rangle$ (more discussions are given below).

In the resonating plaquette phase, the bond-bond correlation functions should have peaks in momentum space

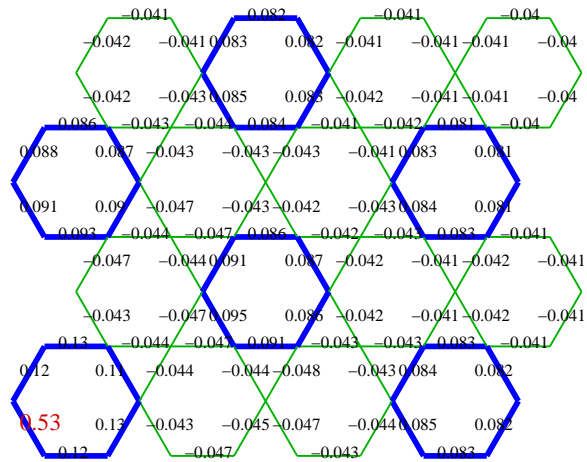


FIG. 2: (color online). The correlation function $C_b(\mathbf{r}_1 - \mathbf{r}_\delta)$ between the bond indicated by a large text (red online) and the other bonds for $L = 24$, $J_z/J_\perp = 10$, $D/J_z = 0.4$, and $T = J_\perp/48$. Resonating hexagons are denoted by thick lines.

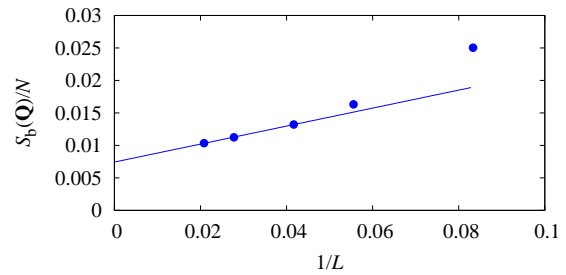


FIG. 3: (color online). Finite size scaling of the equal time bond-bond structure factor $S_b(\mathbf{Q}_0)$ for $L = 24$, $J_z/J_\perp = 10$, $D/J_z = 0.4$, and $T = J_\perp/48$. In this and the other structure factor plots, error bars (if not visible) are smaller than the symbol sizes, and the line shows a linear extrapolation to the thermodynamic limit.

corresponding to the specific pattern in real space characterizing plaquette bond order. In Fig. 2, we show the bond-bond correlations function in real space that is given by

$$C_b(\mathbf{r}_\gamma - \mathbf{r}_\delta) = \left\langle \left[\frac{1}{\beta} \int B_{\gamma\tau} d\tau - B_0 \right] \left[\frac{1}{\beta} \int B_{\delta\tau} d\tau - B_0 \right] \right\rangle, \quad (2)$$

where $B_{\alpha(i,j),\tau} = J_\perp(S_i^x S_j^x + S_i^y S_j^y)$ is the off-diagonal bond operator (at imaginary time τ) of the bond α connecting spins i and j , and B_0 denotes the background bond strength. In Fig. 2, one can clearly see the pattern that is compatible with the VBS-H phase. To confirm that the bond order is long-ranged, we show in Fig. 3 the finite size scaling of the equal time bond-bond structure factor $S_b(\mathbf{q})$ at the ordering wavevector $\mathbf{q} = \mathbf{Q}_0 = (4\pi/3, 0)$,

$$S_b(\mathbf{q}) = N \langle B_{\mathbf{q}\tau}^\dagger B_{\mathbf{q}\tau} \rangle, \quad (3)$$

where $B_{\mathbf{q}\tau} = (1/N) \sum_\alpha B_{\alpha\tau} \exp(i\mathbf{q}\mathbf{r}_\alpha)$. Note that the

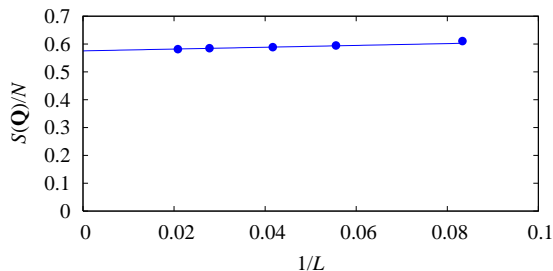


FIG. 4: (color online). Finite size scaling of the equal time spin-spin structure factor $S(\mathbf{Q}_0)$ for $L = 24$, $J_z/J_\perp = 10$, $D/J_z = 0.4$, and $T = J_\perp/48$.

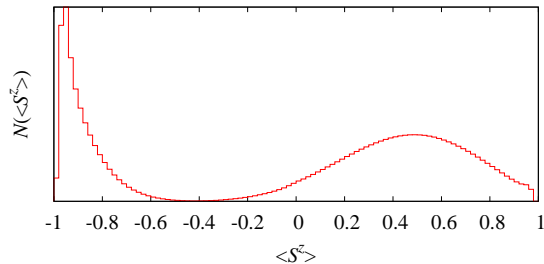


FIG. 5: (color online). Probability distribution (arbitrary units) of \bar{S}_i^z for $L = 48$, $J_z/J_\perp = 10$, $D/J_z = 0.4$, and $T = J_\perp/48$. The distribution function is independent of the system size (not shown).

expression of $B_{\mathbf{q}\tau}$ involves the sum over the bond index α and N is the number of sites. The structure factor divided by the number of sites clearly goes to a finite value in the thermodynamic limit even though the extrapolated value is quite small.

On the other hand, the bond-bond correlation described in the previous paragraph might also be compatible with the FP phase. More robust diagnostic is the distribution function of local $\langle S_i^z \rangle$, which should have two peaks for the VBS-H phase and three peaks for the FP phase if the system is in one of the six degenerate symmetry-broken states.¹⁰ For each Monte Carlo configuration, we compute the time-averaged $\bar{S}_i^z = (1/\beta) \int_0^\beta d\tau S_{i\tau}^z$, $S_{i\tau}^z$ is the z -component of the spin operator at site i and imaginary time τ . In Fig. 5, the distribution function of \bar{S}_i^z is shown. The distribution function has two peaks; one sharp peak at $-b$ and the other broader peak at $b/2$. This is what we expect for the VBS-H phase. For the frozen plaquette phase, one expects three peaks at a , 0 , and $-a$.

The VBS-H phase also has magnetic order. In Fig. 4, we show the finite size scaling of the equal time spin-spin structure factor at $\mathbf{q} = \mathbf{Q}_0$,

$$S(\mathbf{q}) = N \langle S_{\mathbf{q}\tau}^\dagger S_{\mathbf{q}\tau} \rangle, \quad (4)$$

where $S_{\mathbf{q}\tau} = (1/N) \sum_i S_{i\tau}^z \exp(i\mathbf{q}\mathbf{r}_i)$.

Therefore, our Monte Carlo data are consistent with

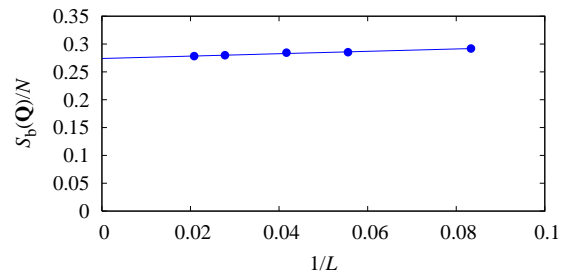


FIG. 6: (color online). Finite size scaling of the equal time bond-bond structure factor $S_b(\mathbf{Q}_3)$ for $J_z/J_\perp = 10.5$, $D = 0$, and $T = J_\perp/12$.

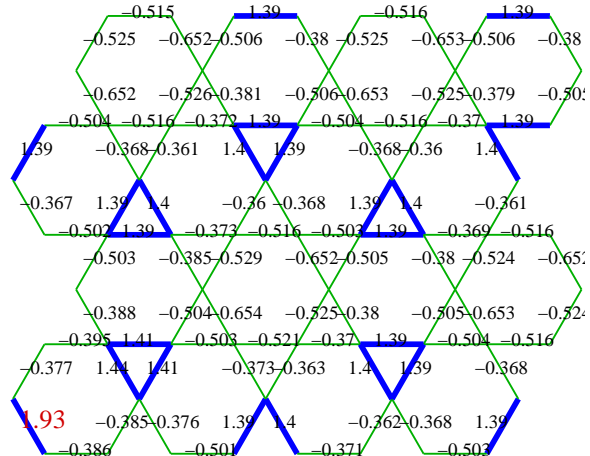


FIG. 7: (color online). The correlation function $C_b(\mathbf{r}_1 - \mathbf{r}_\delta)$ between the bond indicated by a large text (red online) and the other bonds for $L = 12$, $J_z/J_\perp = 10.5$, $D = 0$, and $T = 0.05J_\perp$. Resonating triangles (trimers) are denoted by thick lines.

the resonating plaquette phase (VBS-H). It is worth noting that the VBS-H phase is quite similar to the VBS phase discovered in the hard-core boson model on the kagome lattice at fillings of $1/3$ and $2/3$ (for details, see Ref. 11,12).

B. VBS-T(B) phase

Another interesting result in this work is the discovery of another phase with resonating plaquettes at small values of D/J_\perp and large values of J_z/J_\perp as shown in Fig. 1. This phase was not predicted before. There are actually two different competing phases that are very close in energy. Triangles resonate in one of those phases (VBS-T phase) and bow-ties resonate in the other one (VBS-B phase). We are not able to determine reliably which phase is the true ground state.

We find that there is a finite temperature transition from the high temperature paramagnetic phase to the resonating phase for $J_z/J_\perp \geq 10$ and D close to zero. We have not attempted to obtain the precise location of this

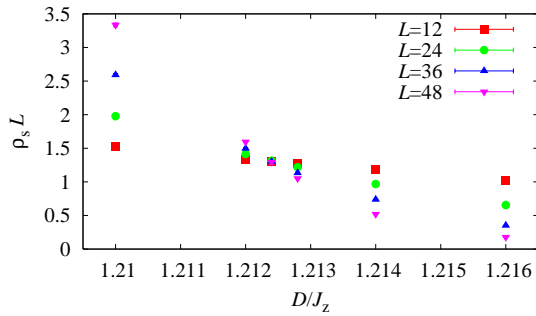


FIG. 10: (color online). Finite size scaling of the superfluid density ρ_s at $J_z/J_\perp = 6$ for $\beta/L = 1/J_\perp$.

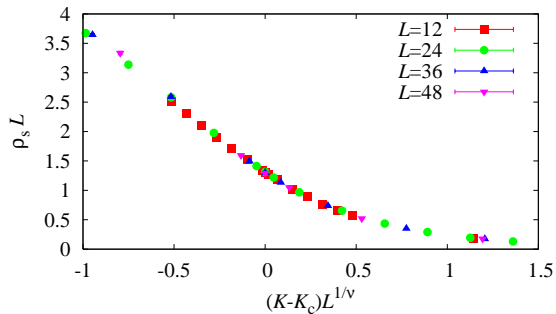


FIG. 11: (color online). Data collapse of the superfluid density ρ_s at $J_z/J_\perp = 6$ for $\beta/L = 1/J_\perp$.

As we have noted above, the bond order is very strong in the VBS-T(B) phase. This may be explained by the fact that the VBS-T phase can be chosen via resonating triangles in first order perturbation theory whereas, in most of other cases (including VBS-H), plaquette resonance is obtained in higher order perturbation theory. As a result, the VBS-T(B) phase may be more robust than other cases.

C. Superfluid-paramagnet phase transition

In this subsection, we discuss the phase transition between the superfluid (or XY ferromagnet in spin language) and the featureless quantum paramagnet. Our numerics shows that this transition is continuous and most likely belongs to the 3d XY universality class. We analyze the finite size scaling of our data as follows. We measure the superfluid density by measuring the winding number fluctuations.¹⁵ In the vicinity of a continuous transition, the superfluid density scales as

$$\rho_s = L^{-z} F_{\rho_s}(L^{1/\nu}(K_c - K), \beta/L^z), \quad (5)$$

where F_{ρ_s} is the scaling function, L is the linear system size, z is the dynamical critical exponent, ν is the correlation length exponent, $K_c - K = (D/J_z)_c - D/J_z$ is the distance to the critical point, and β is the inverse temperature. To cross the phase boundary, we change D and

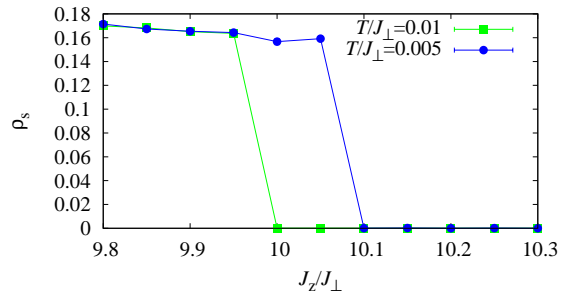


FIG. 12: (color online). The superfluid density ρ_s as a function of J_z/J_\perp for $L = 12$, $D = 0$, and different temperatures. Lines are guides to the eye.

keep J_z fixed. The data scale very well with the dynamical critical exponent $z = 1$. In Fig. 10, the superfluid density ρ_s times the system size L is shown as a function of the coupling constant. As follows from the above scaling form, the curves for different system sizes should cross at the transition point if the ratio β/L^z is fixed. Such a distinct crossing point is seen at $(D/J_z)_c = 1.2124$. It also follows from Eq. 5 that the curves for different system sizes should collapse onto a universal curve for appropriate values of ν and $(D/J_z)_c$ when $\rho_s L$ is plotted as a function of $[(D/J_z)_c - D/J_z]L^{1/\nu}$. In Fig. 11, we show such a data collapse for $\nu = 0.67(2)$ and $(D/J_z)_c = 1.2124(2)$. The error bars are estimated from the stability of the data collapse with respect to varying the fitting parameters. Thus one may conclude that the superfluid-paramagnet quantum phase transition is continuous. One may also infer that the transition is in the 3d XY universality class from $\nu = 0.67(2)$. However, we have not measured the other critical exponents that could be used to unambiguously confirm this prediction.

D. Superfluid-VBS phase transitions

The quantum phase transitions out of the superfluid phase to VBS phases are strongly first order. As an example, let us consider the transition from the superfluid phase to the VBS-T phase. In Fig. 12, we show the superfluid density ρ_s as a function of J_z/J_\perp at different temperatures. The superfluid density jumps at large values of J_z/J_\perp indicating a transition to an insulating phase (VBS-T phase). We confirm that the transition is strongly first order by observing hysteresis effects upon increasing or decreasing J_z/J_\perp across the transition (not shown) and by a double peaked structure in the distribution of the XY energy (kinetic energy of bosons), $J_\perp \langle S_i^x S_j^x + S_i^y S_j^y \rangle$, close to the transition (not shown).

The transition from the superfluid phase to the VBS-H phase is also first order. In the top part of the VBS-H lobe (see Fig. 1), the first order nature becomes somewhat weaker as the value of J_\perp/J_z is decreased. We do not observe a direct transition from the VBS-H phase to

the quantum paramagnetic phase, which was predicted in Ref. 5, in the parameter region we can access, i.e. for $J_{\perp}/J_z \gtrsim 0.08$. There is a narrow region of the superfluid phase between those two phases, as shown in Fig. 1. However, we cannot rule out the possibility that there might be a direct transition at much smaller values of J_{\perp}/J_z .

III. DISCUSSION

We now discuss possible origins of the discrepancy between our quantum Monte Carlo results and those of previous analytic approaches with various approximation schemes.^{4,5,6} In particular, it is found that the VBS-H phase, not the FP, is the stable ground state for moderate strength of D/J_z and small J_{\perp}/J_z . This suggests that the string-net mean field theory analysis in a previous work⁶ may not be sufficient for the identification of the true ground state.

The string-net picture starts from an alternative representation of the spins on the kagome lattice, where the spins are considered to be in the middle of the links connecting the sites of the honeycomb lattice (that can be obtained by connecting the centers of triangles on the kagome lattice).⁶ This honeycomb lattice is a bipartite lattice and consists of A and B sublattices. The occupation of a given link $I = \langle ij \rangle$ by a string is defined as follows; the link contains an oriented string pointing from $i \in A$ to $j \in B$ if $S_I^z = +1$ and from j to i if $S_I^z = -1$. The link is empty if $S_I^z = 0$. Then the spin configurations on the original kagome lattice and those of oriented closed strings are in exact correspondence.⁶

The string-net mean-field theory uses the following ansatz for the variational ground state wavefunction.⁶

$$\Psi_z(X) = \prod_{ij} z_{ij}^{n_{ij}}, \quad (6)$$

where X represents an oriented string configuration and $\{z_{ij}\}$ a large number of variational parameters, and n_{ij}

the occupation number of the oriented link ij . The mean-field analysis begins with a (translationally-invariant) string liquid state (or a string condensed state) where z_{ij} can be set to a constant α . Considering the spectrum of collective modes in this state and the identification of the wavevector where the collective modes become soft, one can in principle study the instability to a translational-symmetry broken state. More explicitly, this can be achieved by writing $z_{ij} = \alpha e^{E_{ij} + iA_{ij}}$ and studying the fluctuations of E_{ij} and A_{ij} . It was found that the soft mode is described by $E = \Phi E_{+\mathbf{Q}} + \Phi^* E_{-\mathbf{Q}}$ and $A = 0$, where $E_{\mathbf{Q}}$ is the Fourier mode at $\mathbf{Q} = (4\pi/3, 0)$ and equivalent wavevectors.⁶ Here Φ is a complex number.

The energy (or the Ginzburg-Landau theory) of the system as a function of Φ can be obtained as^{5,6}

$$H(\Phi) = A|\Phi|^2 + B|\Phi|^4 + C[\Phi^6 + (\Phi^*)^6] + \dots, \quad (7)$$

where A, B, C are real constants and Φ can be regarded as an order parameter. The choice of the ground state is sensitive to the phase of Φ and hence the sign of C basically determines the true ground state. It was found that if C is positive (negative), then the FP (VBS-H) is favored.⁶ This sign, however, is very difficult to determine in analytic approaches. In Ref. 6, an unrestricted variational wavefunction calculation was also done on a small system size 3×3 , leading to the conclusion that the ground state may be the FP phase.⁶ We think, however, that this system size is perhaps too small for definitive conclusion. Indeed our quantum Monte Carlo results are clearly consistent with the VBS-H phase, and hence the negative sign of C in the Ginzburg-Landau theory.

Acknowledgments

This work was supported by the NSERC, CRC, CIFAR, KRF-2005-070-C00044, and the Swiss National Science Foundation (S. V. I.). We thank Cenke Xu, Joel Moore, Michael Levin, Xiao-Gang Wen, and Matthias Troyer for helpful discussions.

¹ For a review of possible quantum phases, see S. Sachdev, *Annales Henri-Poincaré* **4**, 559 (2003).
² L. Balents, M. P. A. Fisher, and S. M. Girvin, *Phys. Rev. B* **65**, 224412(2002); M. Hermele, M. P. A. Fisher, and L. Balents, *Phys. Rev. B* **69**, 064404 (2004).
³ X.-G. Wen, *Phys. Rev. B* **68**, 115413 (2003).
⁴ C. Xu and J. E. Moore, *Phys. Rev. B* **72**, 064455 (2005).
⁵ C. Xu and J. E. Moore, *Phys. Rev. B* **76**, 104427 (2007).
⁶ M. Levin and X.-G. Wen, *Phys. Rev. B* **75**, 075116 (2007).
⁷ A. M. Polyakov, *Nucl. Phys. B* **120**, 429 (1977).
⁸ K. Louis and C. Gros, *Phys. Rev. B* **70**, 100410(R) (2004).
⁹ A. W. Sandvik, *Phys. Rev. B* **59**, R14157 (1999); O. F. Syljuåsen and A. W. Sandvik, *Phys. Rev. E* **66**, 046701 (2002).
¹⁰ On the time scale of our quantum Monte Carlo simulations,

the system stays in one of the six degenerate symmetry-broken states. However, the finite size system should fluctuate between different degenerate states on much longer Monte Carlo time scales.
¹¹ S. V. Isakov, S. Wessel, R. G. Melko, K. Sengupta, Yong Baek Kim, *Phys. Rev. Lett.* **97**, 147202 (2006).
¹² K. Damle and T. Senthil, *Phys. Rev. Lett.* **97**, 067202 (2006).
¹³ K. S. D. Beach, A. W. Sandvik, *Phys. Rev. Lett.* **99**, 047202 (2007).
¹⁴ R. Moessner and S. L. Sondhi, *Phys. Rev. B* **63**, 224401 (2001).
¹⁵ E. L. Pollock and D.M Ceperley, *Phys. Rev. B* **36**, 8343 (1987).